electronics

MDPI

Communication

Using the Uniform Theory of Diffraction to Analyze Radio Wave Propagation along Urban Street Canyons for Device-to-Device Communication

Elena Brugarolas-Ortiz [1], Ignacio Rodríguez-Rodríguez [2], José-Víctor Rodríguez [1,*], Leandro Juan-Llácer [1] and Domingo Pardo-Quiles [1]

[1] Departamento de Tecnologías de la Información y las Comunicaciones, Universidad Politécnica de Cartagena, Antiguo Cuartel de Antigones, Plaza del Hospital, 1, Cartagena, 30202 Murcia, Spain
[2] Departamento de Ingeniería de Comunicaciones, Universidad de Málaga, Avda. Cervantes, 2, 29071 Málaga, Spain
* Correspondence: jvictor.rodriguez@upct.es; Tel.: +34-968-326-548

Abstract: This paper examines the propagation of radio waves in so-called urban street canyons through formulations based on Geometrical Optics (GO) and the Uniform Theory of Diffraction (UTD). As this type of environment comprises a street flanked by tall buildings more or less equally spaced on both sides (creating a canyon-like morphology), estimating the attenuation that radio signals may experience in these scenarios is crucial to the planning of urban device-to-device (D2D) wireless communication. In this sense, the results obtained through the analysis based on GO/UTD (in the horizontal plane containing the transmitter and receiver) are validated by a comparison with experimental measurements, showing good agreement. This work demonstrates how the use of GO/UTD-based formulations can contribute to a simpler and computationally more efficient planning of D2D mobile communication systems in which the considered propagation environment can be modeled as an urban street canyon comprising rectangular and equispaced buildings.

Keywords: street canyons; urban propagation; Geometrical Optics; Uniform Theory of Diffraction; device-to-device communications

Citation: Brugarolas-Ortiz, E.; Rodríguez-Rodríguez, I.; Rodríguez, J.-V.; Juan-Llácer, L.; Pardo-Quiles, D. Using the Uniform Theory of Diffraction to Analyze Radio Wave Propagation along Urban Street Canyons for Device-to-Device Communication. *Electronics* **2023**, *12*, 593. https://doi.org/10.3390/electronics12030593

Academic Editors: Minhoe Kim, Ohyun Jo and Byungchang Chung

Received: 14 December 2022
Revised: 18 January 2023
Accepted: 23 January 2023
Published: 25 January 2023

1. Introduction

With mobile services becoming increasingly vital and big data being integrated into everyday life, the demand for mobile traffic services that offer high data rates is only set to increase. Against this backdrop and with high densities of device users, it seems pertinent to consider device-to-device (D2D) communication, i.e., bypassing the conventional cellular infrastructure when appropriate devices are nearby. In contrast to rooftop cellular networks, since the mobile terminals have direct communication links, the transmitters and receivers of D2D systems are typically located at street level (i.e., the antennae are lower, generally below the rooftops) [1–3]. As a result, conventional propagation models are not adequate for predicting the specific parameters of radio channels in these scenarios. This highlights the need to develop new channel models that consider low-height antennas, especially in urban street canyons, i.e., streets flanked by tall, approximately equispaced structures on either side that produce a canyon-like effect.

The numerous efforts seeking to predict radio wave propagation within urban street canyons have led to the development of a variety of models. For example, [4] first proposed a path loss model to predict propagation in such urban street canyons. The authors hereby considered various regions separately in their theoretical analysis, specifically the line-of-sight (LOS) region, the sudden corner attenuation region, and the non-line-of-sight (NLOS) region. This original diffraction model was further developed by [5] to consider by-four corners, with [6] going on to propose an alternative model that parameterizes

the corner distance, corner loss, and attenuation coefficient. Finally, multiple-diffraction along the horizontal plane in street canyon-like scenarios was analyzed in [7,8] using the Parabolic Equation Model (PEM) with Recursive Convolution Nonlocal Boundary Conditions (PEM-RCNBC).

The above-mentioned models are generally complex from a theoretical point of view and, consequently, are computationally demanding. Therefore, in this work, D2D radio wave propagation within urban street canyons is analyzed in the horizontal plane using straightforward, mathematically simple, and computationally efficient Geometrical Optics (GO) [9] and, in particular, the Uniform Theory of Diffraction (UTD) [10]. Different typical scenarios are hereby evaluated, and the obtained results are properly compared with measurements.

2. Considered Scenarios and Theoretical Analysis

Three different scenarios modeling a simplified street canyon (including both LOS and NLOS situations) are analyzed in the horizontal plane using GO/UTD-based formulations, so that contributions from direct and reflected rays (if applicable), as well as contributions from single, double, triple, and quadruple diffractions, are considered at the receiver. In this sense, the rectangular obstacles that comprise the analyzed environment are assumed to be infinitely high, and thus the effects in the vertical plane can be ignored. Moreover, as the analyzed schemes are symmetrical in the horizontal plane with respect to the central longitudinal axis of the street, only the contributions of one of the two symmetrical sides are assessed. Consequently, to obtain the total signal that reaches the receiving point, a replica of all considered contributions is later added, taking into account those corresponding to the other side. The scenarios considered, as well as the theoretical development carried out through GO/UTD-based formulations, are shown below.

2.1. LOS Case

Figure 1 shows the scheme of the first scenario analyzed, which in this case represents an LOS situation in a street canyon comprising two perfectly conducting rectangular blocks on each side. The figure shows the transmitter point (Tx) and the line (ω) along which the different receiver points (Rx) are located. In addition, the different distance parameters that are taken into account when developing the GO/UTD formulations are also shown. In the following subsections, the expressions of the different contributions reaching the receiver are obtained.

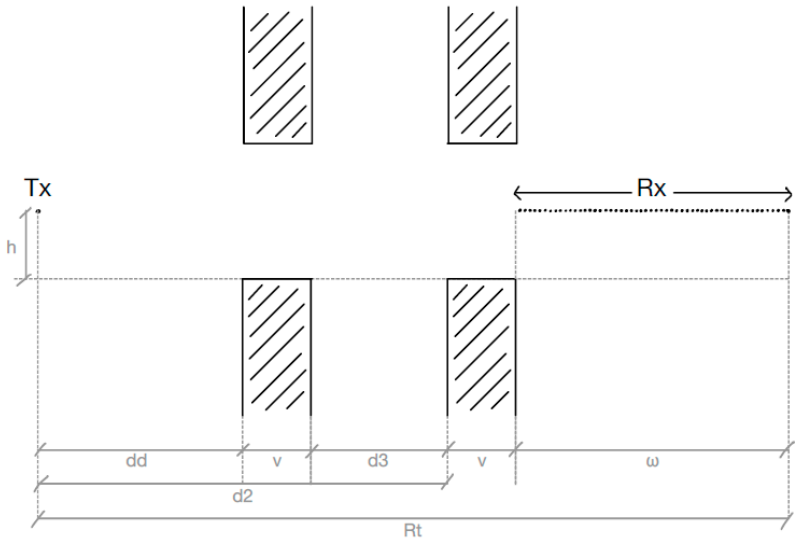

Figure 1. Scheme of the considered LOS scenario.

2.1.1. Direct Ray

In Figure 2, the contribution of the direct ray (Edir) is shown in blue.

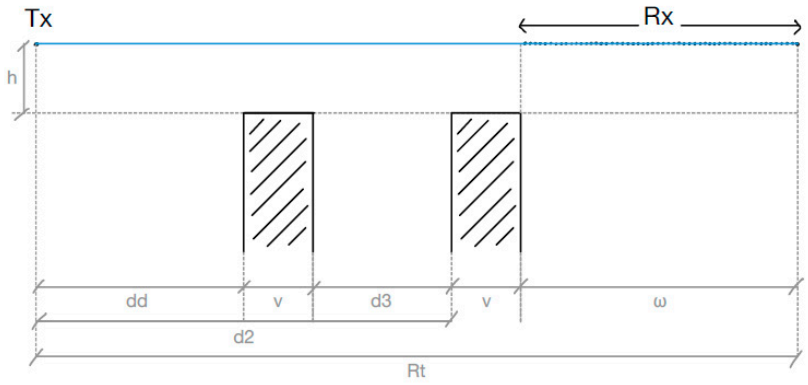

Figure 2. Direct ray contribution of the considered LOS scenario.

Thus, its expression is:

$$Edir = \frac{E0}{Rt} e^{-jkRt} \tag{1}$$

where $E0$ is the relative amplitude of a spherical wave and k is the wave number.

2.1.2. Single Diffractions

In Figures 3–6, the four possible single diffractions between the Tx and Rx (Edif1, Edif2, Edif3, and Edif4) can be observed, considering only the lower side of the street canyon propagation scheme. The GO/UTD expressions for each contribution are given below.

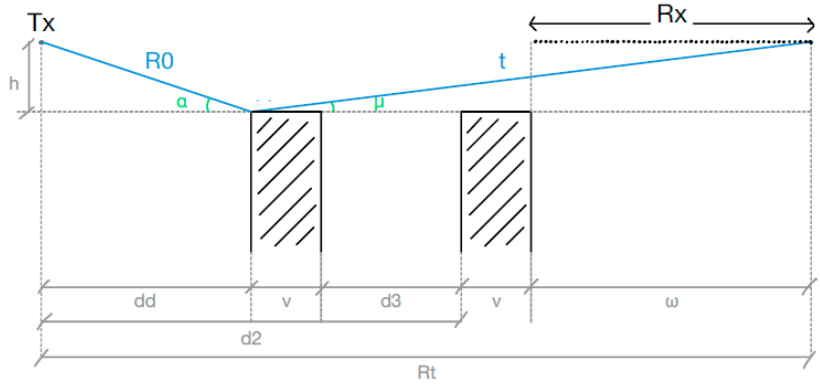

Figure 3. First single diffraction (Edif1) of the considered LOS scenario.

$$Edif1 = \frac{E0}{R0} e^{-jkR0} D\left(\varphi' = \frac{\pi}{2} + \alpha; \varphi = \frac{3\pi}{2} - \mu; L = \frac{R0t}{R0 + t}\right) \sqrt{\frac{R0}{t(R0 + t)}} e^{-jkt} \tag{2}$$

where $D(\varphi', \varphi, L)$ is the UTD diffraction coefficient for a perfectly conducting wedge [11].

$$Edif2 = \frac{E0}{R1} e^{-jkR1} D\left(\varphi' = \beta; \varphi = \pi - \rho; L = \frac{R1z}{R1 + z}\right) \sqrt{\frac{R1}{z(R1 + z)}} e^{-jkz} \tag{3}$$

$$Edif3 = \frac{E0}{R0'} e^{-jkR0'} D\left(\varphi' = \frac{\pi}{2} + \alpha';\ \varphi = \frac{3\pi}{2} - \mu'; L = \frac{R0'p}{R0' + p}\right) \sqrt{\frac{R0'}{p(R1 + p)}} e^{-jkp} \tag{4}$$

$$Edif4 = \frac{E0}{R1'} e^{-jkR1'} D\left(\varphi' = \beta'; \varphi = \pi - \rho'; L = \frac{R1'l}{R1' + l}\right) \sqrt{\frac{R1'}{l(R1' + l)}} e^{-jkl} \tag{5}$$

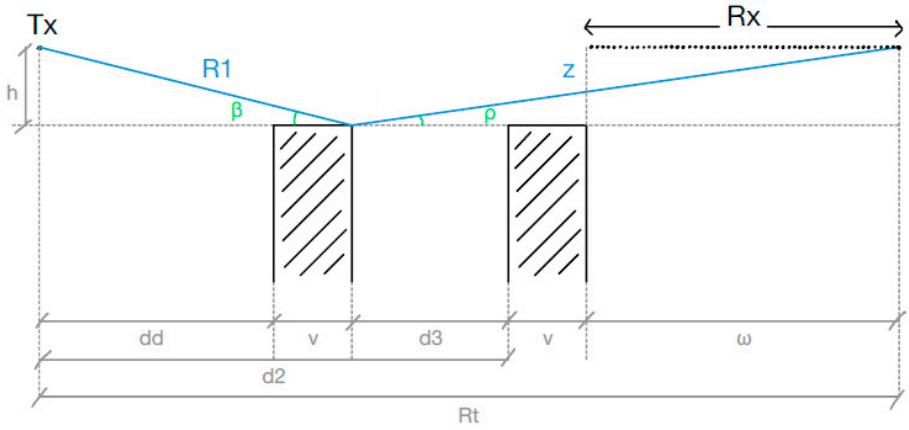

Figure 4. Second single diffraction (Edif2) of the considered LOS scenario.

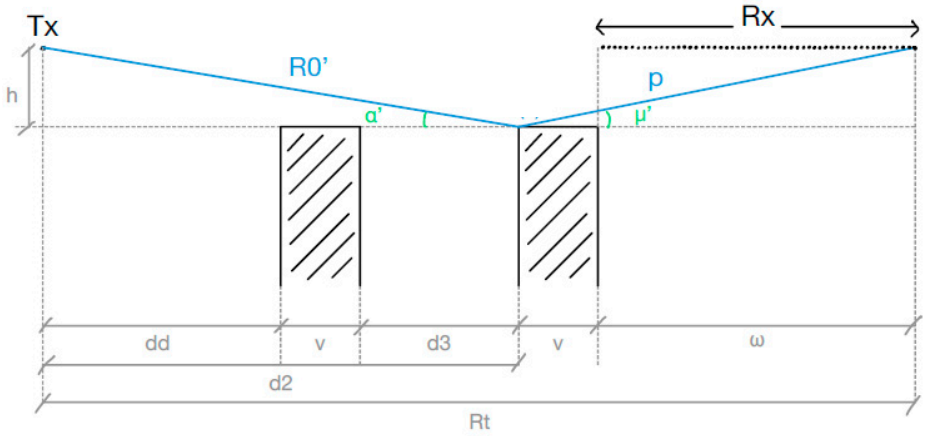

Figure 5. Third single diffraction (Edif3) of the considered LOS scenario.

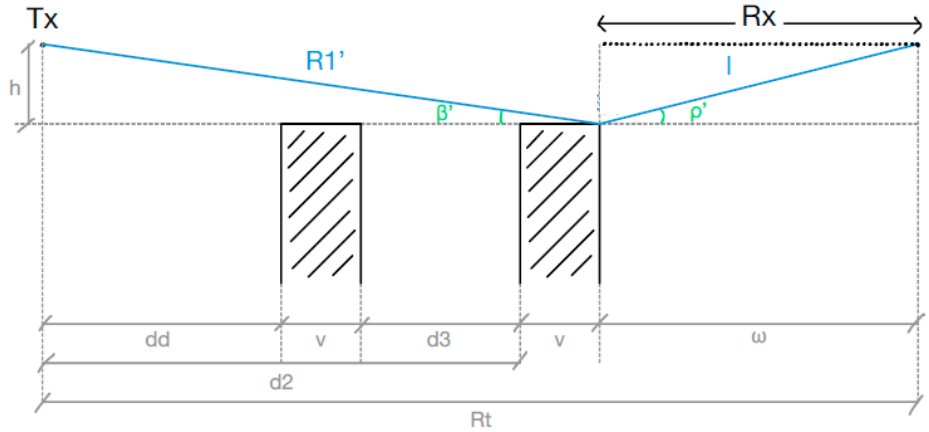

Figure 6. Fourth single diffraction (Edif4) of the considered LOS scenario.

2.1.3. Double Diffractions

In this case, the double diffractions considered (Edif_d1, Edif_d2, Edif_d3, and Edif_d4) are shown in Figures 7–9. The GO/UTD expressions for each contribution are also shown.

$$Edif\_d1 = E(1)D\left(\varphi' = 0; \varphi = \pi - \rho; L = \frac{(R0+v)z}{R0+v+z}\right)\sqrt{\frac{R0+v}{z(R0+v+z)}}e^{-jkz} \quad (6)$$

where

$$E(1) = \frac{E0}{R0} e^{-jkR0} D\left(\varphi' = \frac{\pi}{2} + \alpha; \varphi = \frac{3\pi}{2}; L = \frac{R0v}{R0+v}\right) \sqrt{\frac{R0}{v(R0+v)}} e^{-jkv} \quad (7)$$

$$Edif\_d2 = E(1) D\left(\varphi' = 0; \varphi = \frac{3\pi}{2} - \mu'; L = \frac{(R1+d3)p}{R1+d3+p}\right) \sqrt{\frac{R1+d3}{p(R1+d3+p)}} e^{-jkp} \quad (8)$$

with

$$E(1) = \frac{E0}{R1} e^{-jkR1} D\left(\varphi' = \beta; \varphi = \pi; L = \frac{R1d3}{R1+d3}\right) \sqrt{\frac{R1}{d3(R1+d3)}} e^{-jkd3} \quad (9)$$

$$Edif\_d3 = E(1) D\left(\varphi' = 0; \varphi = \pi - \rho'; L = \frac{(R0'+v)l}{R0'+v+l}\right) \sqrt{\frac{R0'+v}{l(R0'+v+l)}} e^{-jkl} \quad (10)$$

where

$$E(1) = \frac{E0}{R0'} e^{-jkR0'} D\left(\varphi' = \frac{\pi}{2} + \alpha'; \varphi = \frac{3\pi}{2}; L = \frac{R0'v}{R0'+v}\right) \sqrt{\frac{R0'}{v(R0'+v)}} e^{-jkv} \quad (11)$$

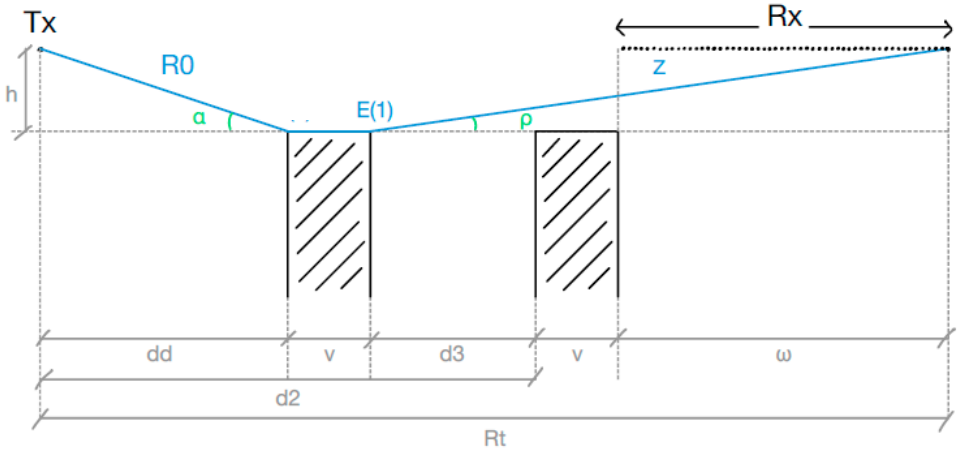

Figure 7. First double diffraction (Edif_d1) of the considered LOS scenario.

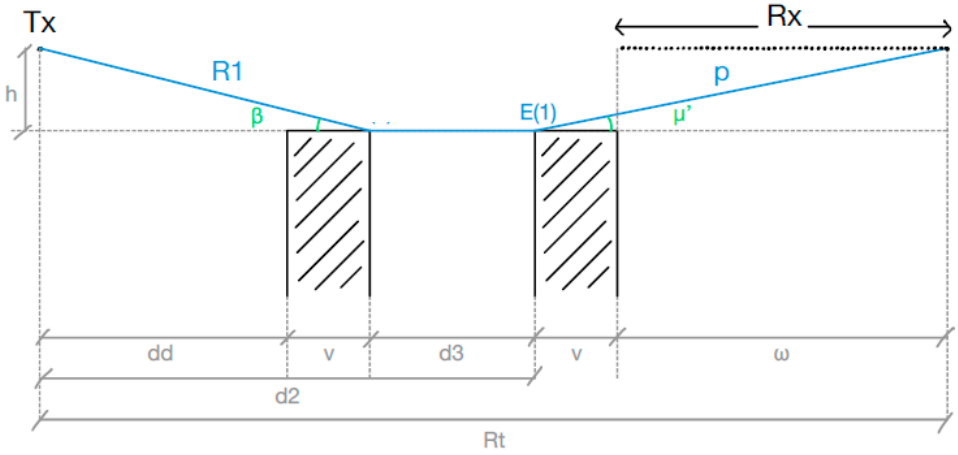

Figure 8. Second double diffraction (Edif_d2) of the considered LOS scenario.

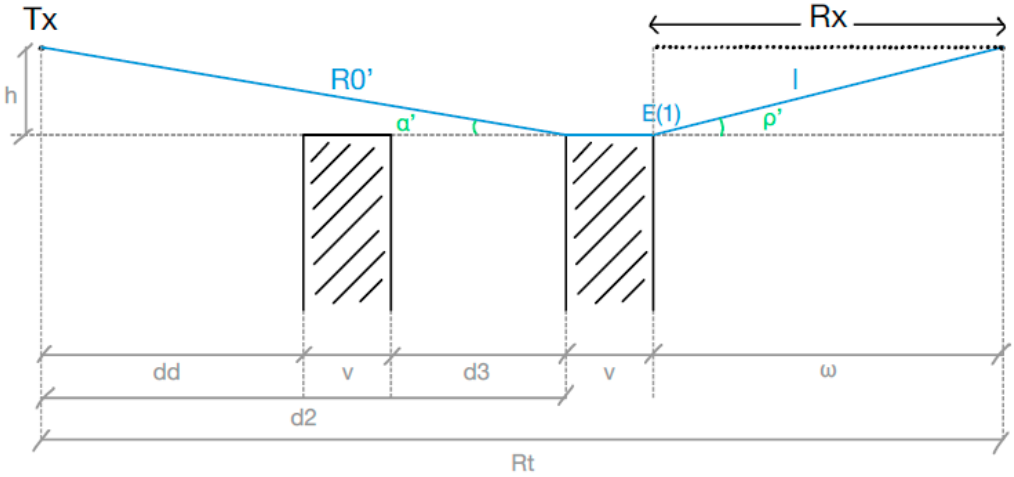

Figure 9. Third double diffraction (Edif_d3) of the considered LOS scenario.

2.1.4. Triple Diffractions

Similarly, Figures 10 and 11 show the triple diffractions considered (Edif_t1 and Edif_t2), with their GO/UTD expressions shown below.

$$Edif\_t1 = E(2)D\left(\varphi' = 0; \varphi = \frac{3\pi}{2} - \mu'; L = \frac{(R0 + v + d3)p}{R0 + v + d3 + p}\right)\sqrt{\frac{R0 + v + d3}{p(R0 + v + d3 + p)}}e^{-jkp} \tag{12}$$

where

$$E(2) = E(1)D\left(\varphi' = 0; \varphi = \pi; L = \frac{(R0 + v)d3}{R0 + v + d3}\right)\sqrt{\frac{R0 + v}{d3(R0 + v + d3)}}e^{-jkd3} \tag{13}$$

$$E(1) = \frac{E0}{R0}e^{-jkR0}D\left(\varphi' = \frac{\pi}{2} + \alpha; \varphi = \frac{3\pi}{2}; L = \frac{R0v}{R0 + v}\right)\sqrt{\frac{R0}{v(R0 + v)}}e^{-jkv} \tag{14}$$

$$Edif\_t2 = E(2)D\left(\varphi' = 0; \varphi = \pi - \rho'; L = \frac{(R1 + d3 + v)l}{R1 + d3 + v + l}\right)\sqrt{\frac{R1 + d3 + v}{l(R1 + d3 + v + l)}}e^{-jkl} \tag{15}$$

with

$$E(2) = E(1)D\left(\varphi' = 0; \varphi = \frac{3\pi}{2}; L = \frac{(R1 + d3)v}{R1 + d3 + v}\right)\sqrt{\frac{R1 + d3}{v(R1 + d3 + v)}}e^{-jkv} \tag{16}$$

$$E(1) = \frac{E0}{R1}e^{-jkR1}D\left(\varphi' = \beta; \varphi = \pi; L = \frac{R1d3}{R1 + d3}\right)\sqrt{\frac{R1}{d3(R1 + d3)}}e^{-jkd3} \tag{17}$$

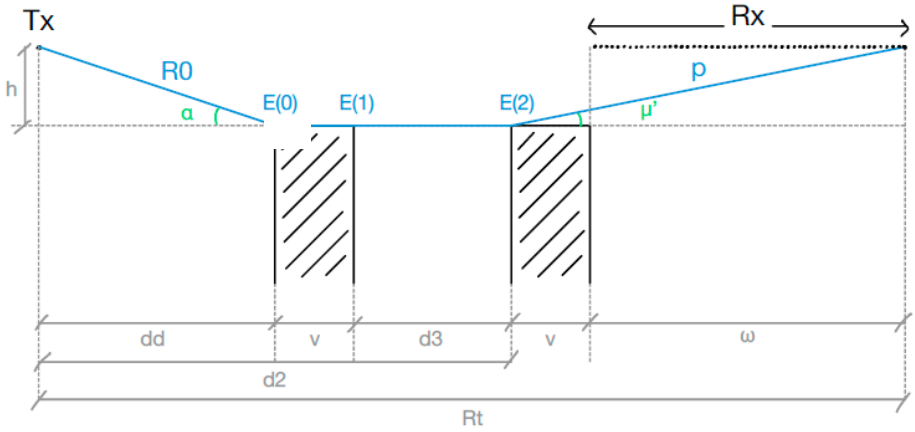

Figure 10. First triple diffraction (Edif_t1) of the considered LOS scenario.

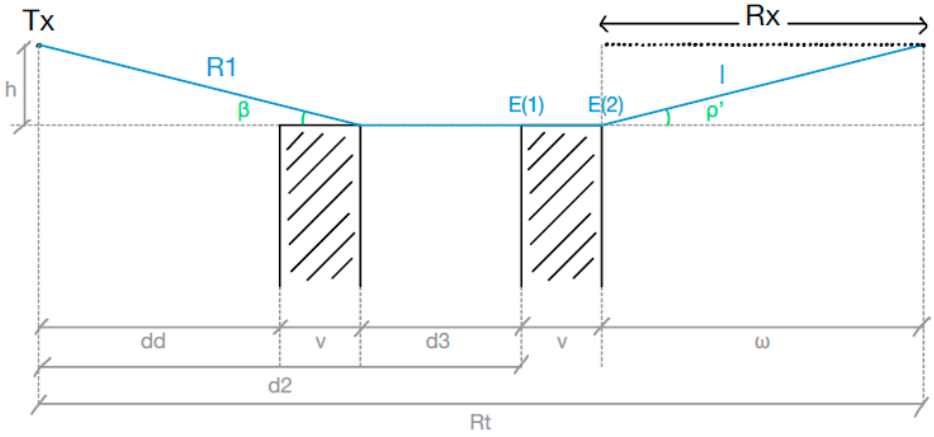

Figure 11. Second triple diffraction (Edif_t2) of the considered LOS scenario.

2.1.5. Quadruple Diffractions

On the other hand, Figure 12 shows the contribution diffracted on the four corners of the two rectangular blocks considered (Edif_q). In this sense, the GO/UTD expression is shown below.

$$Edif\_q = E(3)D\left(\varphi' = 0; \varphi = \pi - \rho'; L = \frac{(R0 + 2v + d3)l}{R0 + 2v + d3 + l}\right)\sqrt{\frac{R0 + 2v + d3}{l(R0 + 2v + d3 + l)}}e^{-jkl} \quad (18)$$

where

$$E(3) = E(2)D\left(\varphi' = 0; \varphi = \frac{3\pi}{2}; L = \frac{(R0 + v + d3)v}{R0 + v + d3 + v}\right)\sqrt{\frac{R0 + v + d3}{v(R0 + v + d3 + v)}}e^{-jkv} \quad (19)$$

$$E(2) = E(1)D\left(\varphi' = 0; \varphi = \pi; L = \frac{(R0 + v)d3}{R0 + v + d3}\right)\sqrt{\frac{R0 + v}{d3(R0 + v + d3)}}e^{-jkd3} \quad (20)$$

$$E(1) = \frac{E0}{R0}e^{-jkR0}D\left(\varphi' = \frac{\pi}{2} + \alpha; \varphi = \frac{3\pi}{2}; L = \frac{R0v}{R0 + v}\right)\sqrt{\frac{R0}{v(R0 + v)}}e^{-jkv} \quad (21)$$

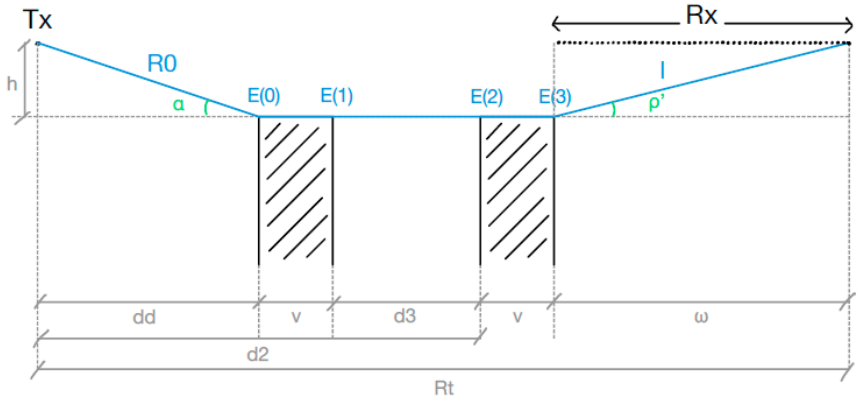

Figure 12. Quadruple diffraction (Edif_q) of the considered LOS scenario.

2.1.6. Reflected Rays

Finally, in Figures 13 and 14 (not to scale), we can observe the groups of rays reflected on the two obstacles (Eref1 and Eref2, respectively), whose GO expressions are shown below.

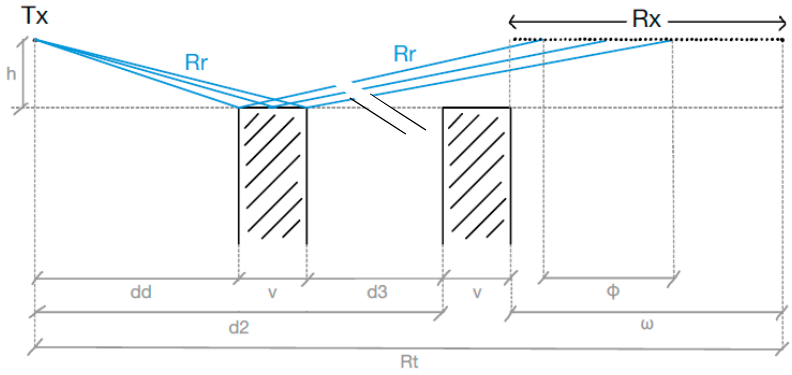

Figure 13. Reflected rays over the first obstacle (Eref1) of the considered LOS scenario.

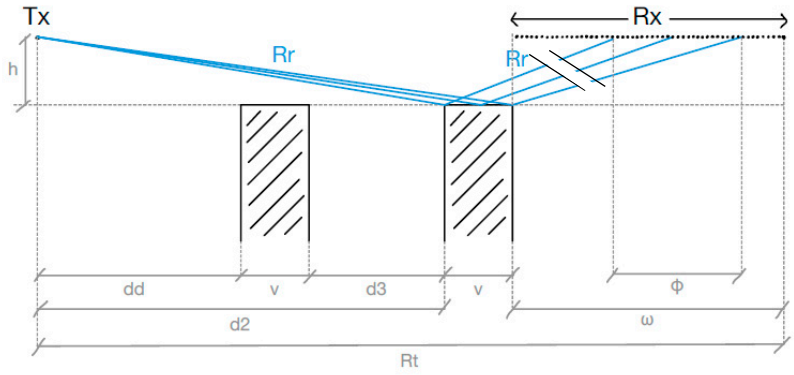

Figure 14. Reflected rays over the second obstacle (Eref2) of the considered LOS scenario.

$$Eref1 = \sum_{0}^{\phi} \frac{E0}{2Rr} Re^{-jk2Rr} = \sum_{0}^{\phi} \frac{E0}{2Rr} e^{-jk2Rr} \tag{22}$$

where R is the reflection coefficient for a perfectly conducting surface (R = 1 for vertical/*hard* polarization and R = −1 for horizontal/*soft* polarization).

$$Eref2 = \sum_{0}^{\phi} \frac{E0}{2Rr'} Re^{-jk2Rr'} = \sum_{0}^{\phi} \frac{E0}{2Rr'} e^{-jk2Rr'} \tag{23}$$

2.1.7. Total Signal

Therefore, the total signal at the receiver, taking into account all the contributions (considering also the upper part of the street canyon), is

$$Et = Edir + 2(Edif1 + Edif2 + Edif3 + Edif4 + Edif\_d1 + Edif\_d2 + Edif\_d3 + Edif\_t1 + Edif\_t2 + Edif\_q + Eref1 + Eref2) \quad (24)$$

2.2. First NLOS Case

Figure 15 shows the scheme of the second scenario analyzed, which in this case represents an NLOS situation in a distribution comprising two perfectly conducting rectangular blocks located right in the middle of the path between Tx and Rx. In the following subsections, the GO/UTD expressions of the different contributions reaching the receiver are obtained.

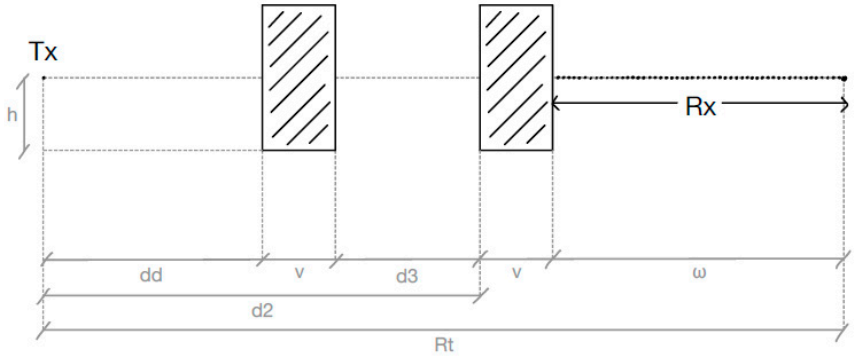

Figure 15. Scheme of the first considered NLOS scenario.

2.2.1. Quadruple Diffraction

Figure 16 shows the considered quadruple diffraction (Edif_q), followed by its GO/UTD expression.

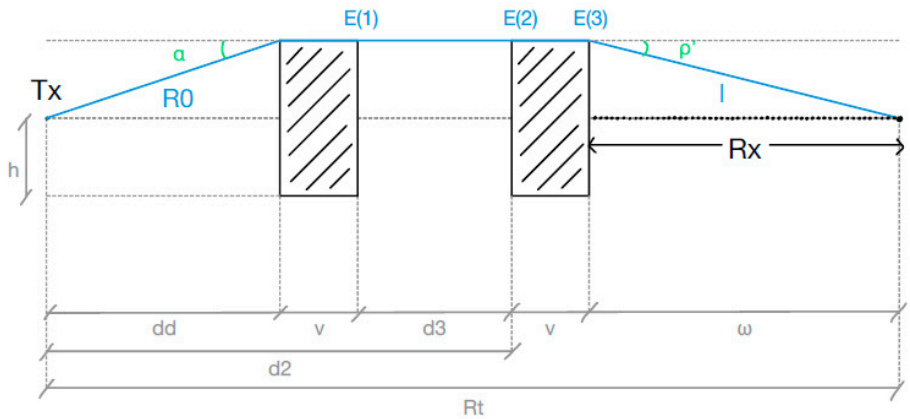

Figure 16. Quadruple diffraction (Edif_q) of the first considered NLOS scenario.

$$Edif\_q = E(3)D\left(\varphi' = 0; \varphi = \pi + \rho'; L = \frac{(R0 + 2v + d3)l}{R0 + 2v + d3 + l}\right)\sqrt{\frac{R0 + 2v + d3}{l(R0 + 2v + d3 + l)}}e^{-jkl} \quad (25)$$

where

$$E(3) = E(2)D\left(\varphi' = 0; \varphi = \frac{3\pi}{2}; L = \frac{(R0 + d3 + v)v}{R0 + d3 + 2v}\right)\sqrt{\frac{R0 + d3 + v}{v(R0 + d3 + 2v)}}e^{-jkv} \quad (26)$$

$$E(2) = E(1)D\left(\varphi' = 0; \varphi = \pi; L = \frac{(R0+v)d3}{R0+v+d3}\right)\sqrt{\frac{R0+v}{d3(R0+2v+d3)}}e^{-jkd3} \quad (27)$$

$$E(1) = \frac{E0}{R0}e^{-jkR0}D\left(\varphi' = \frac{\pi}{2} - \alpha; \varphi = \frac{3\pi}{2}; L = \frac{R0v}{R0+v}\right)\sqrt{\frac{R0}{v(R0+v)}}e^{-jkv} \quad (28)$$

2.2.2. Total Signal

Therefore, in this case, the total signal at the receiver, taking into account that only the contribution of the quadruple diffraction is considered and also adding the one corresponding to the lower part of the street canyon, is

$$Et = 2Edif\_q \quad (29)$$

2.3. Second NLOS Case

Finally, Figure 17 shows the scheme of the third scenario analyzed, where, in this case, perfectly conducting rectangular blocks located on both sides of the path between Tx and Rx and in between (NLOS situation) are combined. In the following subsections, the GO/UTD expressions of the different contributions reaching the receiver are developed.

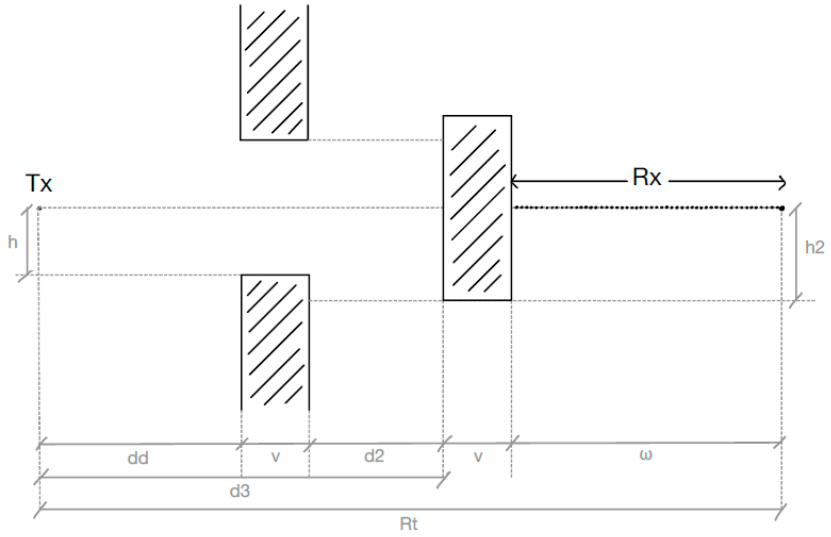

Figure 17. Scheme of the second considered NLOS scenario.

2.3.1. Double Diffraction

Figure 18 shows the double diffraction considered (Edif_d). Its GO/UTD expression is shown below.

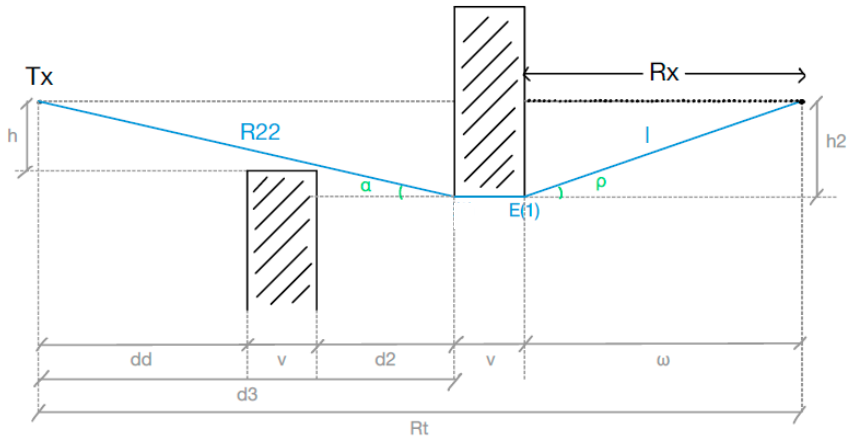

Figure 18. Double diffraction (Edif_d) of the second considered NLOS scenario.

$$Edif\_d = E(1)D\left(\varphi' = 0; \varphi = \pi + \rho; L = \frac{(R22 + v)l}{R22 + v + l}\right)\sqrt{\frac{R22 + v}{l(R22 + v + l)}}e^{-jkl} \quad (30)$$

where

$$E(1) = \frac{E0}{R22}e^{-jkR22}D\left(\varphi' = \frac{\pi}{2} - \alpha; \varphi = \frac{3\pi}{2}; L = \frac{R22v}{R22 + v}\right)\sqrt{\frac{R22}{v(R22 + v)}}e^{-jkv} \quad (31)$$

2.3.2. Triple Diffractions

Likewise, in Figures 19–21, the triple diffractions considered (Edif_t1, Edif_t2, and Edif_t3) can be observed. Their GO/UTD expressions are shown below.

$$Edif\_t1 = E(2)D\left(\varphi' = 0; \varphi = \pi + \rho; L = \frac{(R1 + R3 + v)l}{R1 + R3 + v + l}\right)\sqrt{\frac{R1 + R3 + v}{l(R1 + R3 + v + l)}}e^{-jkl} \quad (32)$$

where

$$E(2) = E(1)D\left(\varphi' = \frac{\pi}{2} - \tau; \varphi = \frac{3\pi}{2}; L = \frac{(R1 + R3)v}{R1 + R3 + v}\right)\sqrt{\frac{R1 + R3}{v(R1 + R3 + v)}}e^{-jkv} \quad (33)$$

$$E(1) = \frac{E0}{R1}e^{-jkR1}D\left(\varphi' = \beta; \varphi = \pi + \tau; L = \frac{R1R3}{R1 + R3}\right)\sqrt{\frac{R1}{R3(R1 + R3)}}e^{-jkR3} \quad (34)$$

$$Edif\_t2 = E(2)D\left(\varphi' = 0; \varphi = \pi + \rho; L = \frac{(R0 + R4 + v)l}{R0 + R4 + v + l}\right)\sqrt{\frac{R0 + R4 + v}{l(R0 + R4 + v + l)}}e^{-jkl} \quad (35)$$

with

$$E(2) = E(1)D\left(\varphi' = \frac{\pi}{2} - \Omega; \varphi = \frac{3\pi}{2}; L = \frac{(R0 + R4)v}{R0 + R4 + v}\right)\sqrt{\frac{R0 + R4}{v(R0 + R4 + v)}}e^{-jkv} \quad (36)$$

$$E(1) = \frac{E0}{R0}e^{-jkR0}D\left(\varphi' = \frac{\pi}{2} + \beta'; \varphi = \frac{3\pi}{2} - \Omega; L = \frac{R0R4}{R0 + R4}\right)\sqrt{\frac{R0}{R4(R0 + R4)}}e^{-jkR4} \quad (37)$$

$$Edif\_t3 = E(2)D\left(\varphi' = 0; \varphi = \pi + \rho; L = \frac{(R1 + R5 + v)l}{R1 + R5 + v + l}\right)\sqrt{\frac{R1 + R5 + v}{l(R1 + R5 + v + l)}}e^{-jkl} \quad (38)$$

where

$$E(2) = E(1)D\left(\varphi' = \frac{\pi}{2} - \theta; \varphi = \frac{3\pi}{2}; L = \frac{(R1 + R5)v}{R4 + R5 + v}\right)\sqrt{\frac{R1 + R5}{v(R1 + R5 + v)}}e^{-jkv} \quad (39)$$

$$E(1) = \frac{E0}{R1}e^{-jkR1}D\left(\varphi' = \beta; \varphi = \pi - \theta; L = \frac{R1R5}{R0 + R4}\right)\sqrt{\frac{R1}{R5(R1 + R5)}}e^{-jkR5} \quad (40)$$

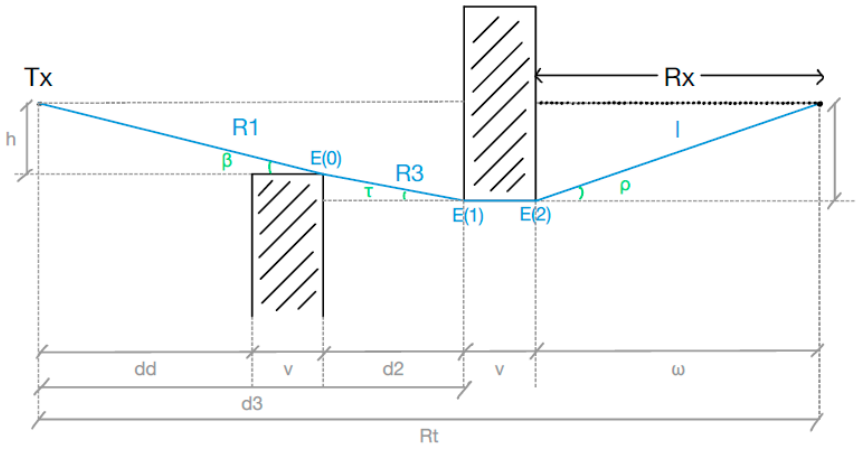

Figure 19. First triple diffraction (Edif_t1) of the second considered NLOS scenario.

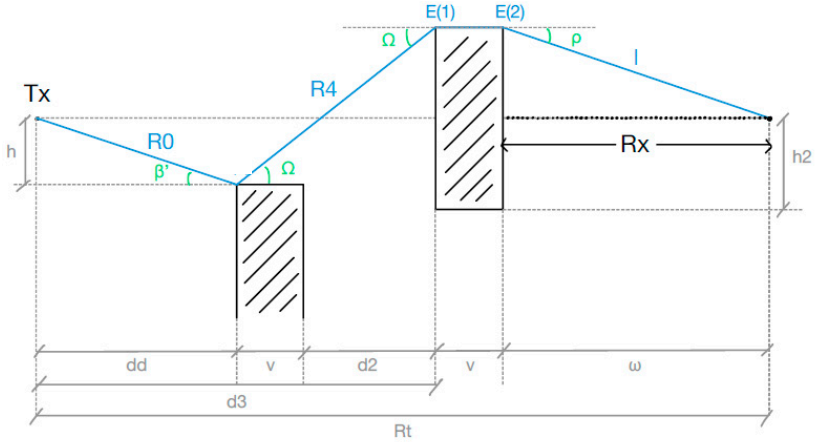

Figure 20. Second triple diffraction (Edif_t2) of the second considered NLOS scenario.

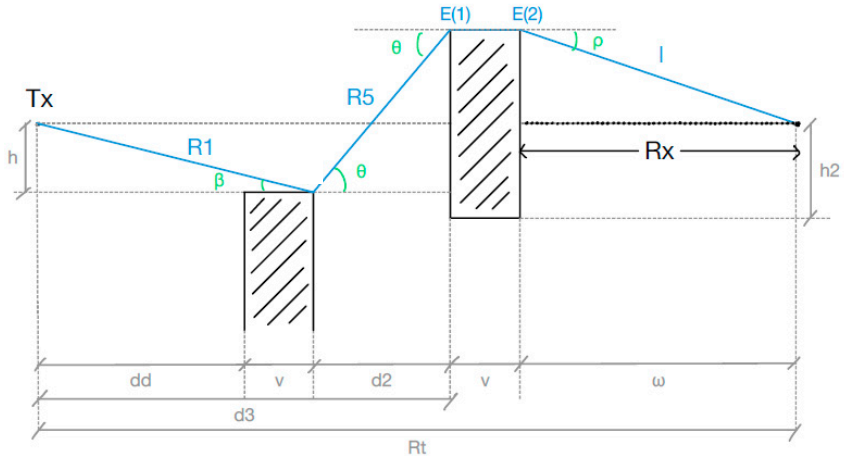

Figure 21. Third triple diffraction (Edif_t3) of the second considered NLOS scenario.

2.3.3. Quadruple Diffractions

Finally, Figures 22–27 show the contributions that have been diffracted four times over the rectangular blocks of the considered scenario (Edif_q1, Edif_q2, Edif_q3, and Edif_q4). Their GO/UTD expressions are presented below.

$$Edif\_q1 = E(3)D\left(\varphi' = 0; \varphi = \pi + \rho; L = \frac{(R0 + 2v + R3)l}{R0 + 2v + R3 + l}\right)\sqrt{\frac{R0 + 2v + R3}{l(R0 + 2v + R3 + l)}}e^{-jkl} \quad (41)$$

where

$$E(3) = E(2)D\left(\varphi' = \frac{\pi}{2} - \tau; \varphi = \frac{3\pi}{2}; L = \frac{(R0 + R3 + v)v}{R0 + R3 + 2v}\right)\sqrt{\frac{R0 + R3 + v}{v(R0 + R3 + 2v)}}e^{-jkv} \tag{42}$$

$$E(2) = E(1)D\left(\varphi' = 0; \varphi = \pi + \tau; L = \frac{(R0 + v)R3}{R0 + v + R3}\right)\sqrt{\frac{R0 + v}{R3(R0 + v + R3)}}e^{-jkR3} \tag{43}$$

$$E(1) = \frac{E0}{R0}e^{-jkR0}D\left(\varphi' = \frac{\pi}{2} + \beta'; \varphi = \frac{3\pi}{2}; L = \frac{R0v}{R0 + v}\right)\sqrt{\frac{R0}{v(R0 + v)}}e^{-jkv} \tag{44}$$

$$Edif\_q2 = E(3)D\left(\varphi' = 0; \varphi = \pi + \rho; L = \frac{(R0 + 2v + R5)l}{R0 + 2v + R5 + l}\right)\sqrt{\frac{R0 + 2v + R5}{l(R0 + 2v + R5 + l)}}e^{-jkl} \tag{45}$$

with

$$E(3) = E(2)D\left(\varphi' = \frac{\pi}{2} - \theta; \varphi = \frac{3\pi}{2}; L = \frac{(R0 + R5 + v)v}{R0 + R5 + 2v}\right)\sqrt{\frac{R0 + R5 + v}{v(R0 + R5 + 2v)}}e^{-jkv} \tag{46}$$

$$E(2) = E(1)D\left(\varphi' = 0; \varphi = \pi - \theta; L = \frac{(R0 + v)R5}{R0 + v + R5}\right)\sqrt{\frac{R0 + v}{R5(R0 + v + R5)}}e^{-jkR5} \tag{47}$$

$$E(1) = \frac{E0}{R0}e^{-jkR0}D\left(\varphi' = \frac{\pi}{2} + \beta'; \varphi = \frac{3\pi}{2}; L = \frac{R0v}{R0 + v}\right)\sqrt{\frac{R0}{v(R0 + v)}}e^{-jkv} \tag{48}$$

$$Edif\_q3 = E(3)D\left(\varphi' = 0; \varphi = \pi + \rho; L = \frac{(R1 + R6 + R3 + v)l}{R1 + R6 + R3 + v + l}\right)\sqrt{\frac{R1 + R6 + R3 + v}{l(R1 + R6 + R3 + v + l)}}e^{-jkl} \tag{49}$$

where

$$E(3) = E(2)D\left(\varphi' = \frac{\pi}{2} + \tau; \varphi = \frac{3\pi}{2}; L = \frac{(R1 + R6 + R3)v}{R1 + R6 + R3 + v}\right)\sqrt{\frac{R1 + R6 + R3}{v(R1 + R6 + R3 + v)}}e^{-jkv} \tag{50}$$

$$E(2) = E(1)D\left(\varphi' = \frac{\pi}{2}; \varphi = \pi + \tau; L = \frac{(R1 + R6)R3}{R1 + R6 + R3}\right)\sqrt{\frac{R1 + R6}{R3(R1 + R6 + R3)}}e^{-jkR3} \tag{51}$$

$$E(1) = \frac{E0}{R1}e^{-jkR1}D\left(\varphi' = \beta; \varphi = \frac{\pi}{2}; L = \frac{R1R6}{R1 + R6}\right)\sqrt{\frac{R1}{R6(R1 + R6)}}e^{-jkR6} \tag{52}$$

$$Edif\_q4 = E(3)D\left(\varphi' = 0; \varphi = \pi + \rho; L = \frac{(R1 + R6 + R5 + v)l}{R1 + R6 + R5 + v + l}\right)\sqrt{\frac{R1 + R6 + R5 + v}{l(R1 + R6 + R5 + v + l)}}e^{-jkl} \tag{53}$$

with

$$E(3) = E(2)D\left(\varphi' = \frac{\pi}{2} - \theta; \varphi = \frac{3\pi}{2}; L = \frac{(R1 + R6 + R5)v}{R1 + R6 + R5 + v}\right)\sqrt{\frac{R1 + R6 + R5}{v(R1 + R6 + R5 + v)}}e^{-jkv} \tag{54}$$

$$E(2) = E(1)D\left(\varphi' = \frac{\pi}{2}; \varphi = \frac{\pi}{2} + \theta; L = \frac{(R1 + R6)R5}{R1 + R6 + R5}\right)\sqrt{\frac{R1 + R6}{R5(R1 + R6 + R5)}}e^{-jkR5} \tag{55}$$

$$E(1) = \frac{E0}{R1} e^{-jkR1} D\left(\varphi' = \beta; \varphi = \frac{\pi}{2}; L = \frac{R1R6}{R1+R6}\right) \sqrt{\frac{R1}{R6(R1+R6)}} e^{-jkR6} \quad (56)$$

$$Edif\_q5 = E(3) D\left(\varphi' = 0; \varphi = \pi + \rho; L = \frac{(R0+R7+R3+v)l}{R0+R7+R3+v+l}\right) \sqrt{\frac{R0+R7+R3+v}{l(R0+R7+R3+v+l)}} e^{-jkl} \quad (57)$$

where

$$E(3) = E(2) D\left(\varphi' = \frac{\pi}{2} + \tau; \varphi = \frac{3\pi}{2}; L = \frac{(R0+R7+R3)v}{R0+R7+R3+v}\right) \sqrt{\frac{R0+R7+R3}{v(R0+R7+R3+v)}} e^{-jkv} \quad (58)$$

$$E(2) = E(1) D\left(\varphi' = \frac{\pi}{2} - \mu; \varphi = \frac{3\pi}{2} - \tau; L = \frac{(R0+R7)R3}{R0+R7+R3}\right) \sqrt{\frac{R0+R7}{R3(R0+R7+R3)}} e^{-jkR3} \quad (59)$$

$$E(1) = \frac{E0}{R0} e^{-jkR0} D\left(\varphi' = \frac{\pi}{2} + \beta; \varphi = \frac{3\pi}{2} - \mu; L = \frac{R0R7}{R0+R7}\right) \sqrt{\frac{R0}{R7(R0+R7)}} e^{-jkR7} \quad (60)$$

$$Edif\_q6 = E(3) D\left(\varphi' = 0; \varphi = \pi + \rho; L = \frac{(R0+R7+R5+v)l}{R0+R7+R5+v+l}\right) \sqrt{\frac{R0+R7+R5+v}{l(R0+R7+R5+v+l)}} e^{-jkl} \quad (61)$$

with

$$E(3) = E(2) D\left(\varphi' = \frac{\pi}{2} - \theta; \varphi = \frac{3\pi}{2}; L = \frac{(R0+R7+R5)v}{R0+R7+R5+v}\right) \sqrt{\frac{R0+R7+R5}{v(R0+R7+R5+v)}} e^{-jkv} \quad (62)$$

$$E(2) = E(1) D\left(\varphi' = \frac{\pi}{2} - \mu; \varphi = \pi - \theta; L = \frac{(R0+R7)R5}{R0+R7+R5}\right) \sqrt{\frac{R0+R7}{R5(R0+R7+R5)}} e^{-jkR5} \quad (63)$$

$$E(1) = \frac{E0}{R0} e^{-jkR0} D\left(\varphi' = \frac{\pi}{2} + \beta; \varphi = \frac{3\pi}{2} - \mu; L = \frac{R0R7}{R0+R7}\right) \sqrt{\frac{R0}{R7(R0+R7)}} e^{-jkR7} \quad (64)$$

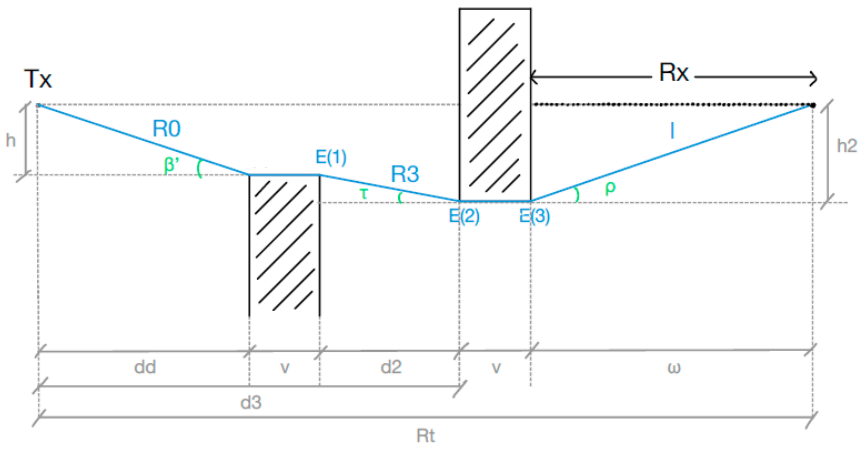

Figure 22. First quadruple diffraction (Edif_q1) of the second considered NLOS scenario.

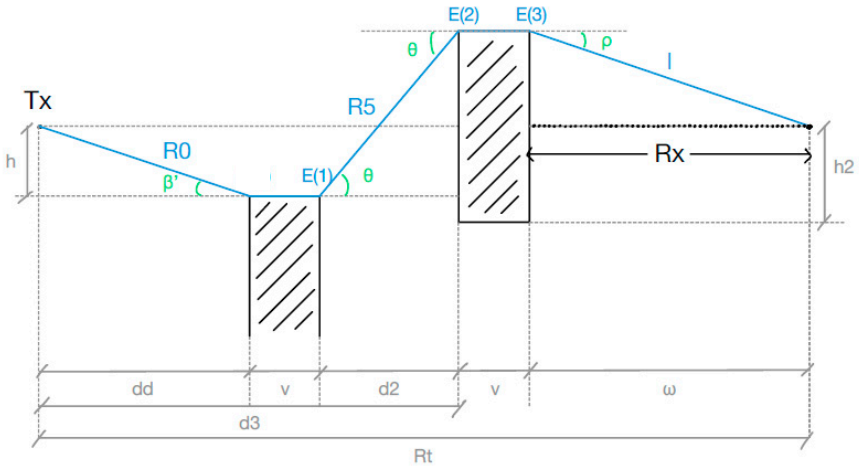

Figure 23. Second quadruple diffraction (Edif_q2) of the second considered NLOS scenario.

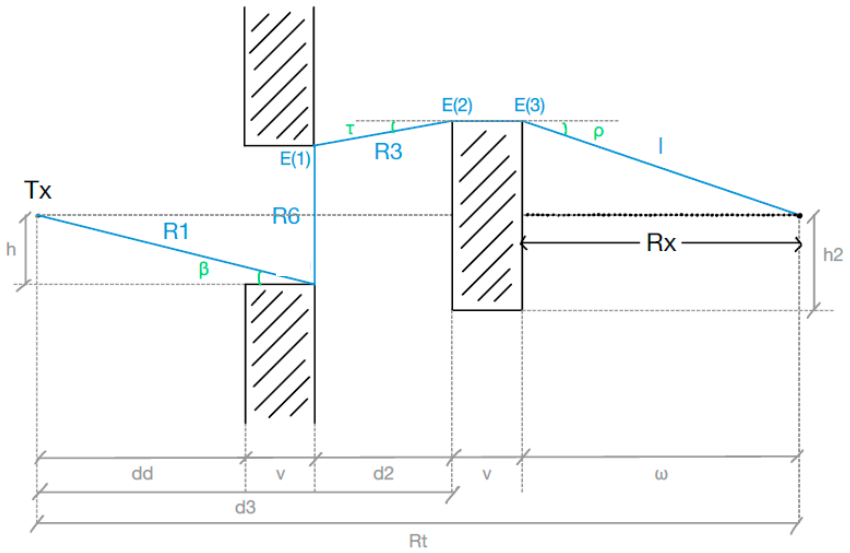

Figure 24. Third quadruple diffraction (Edif_q3) of the second considered NLOS scenario.

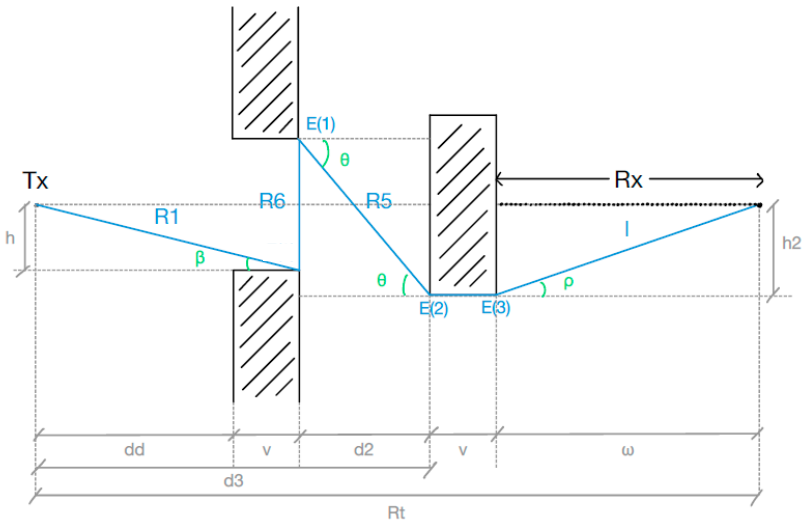

Figure 25. Fourth quadruple diffraction (Edif_q4) of the second considered NLOS scenario.

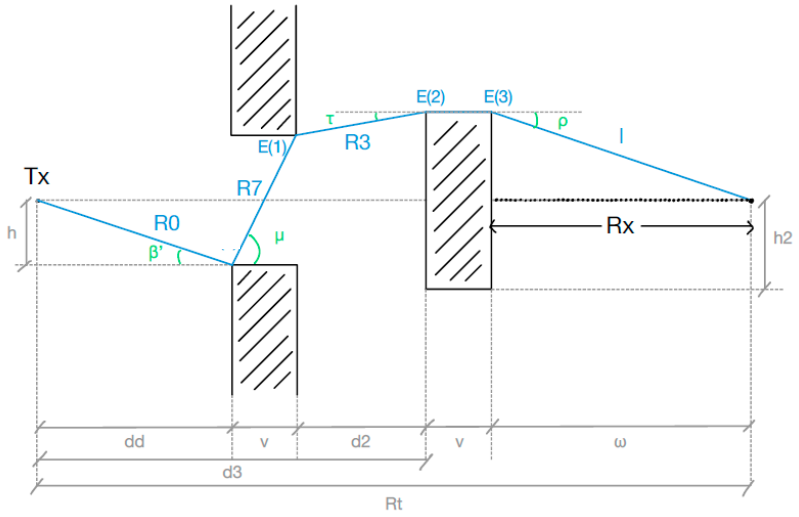

Figure 26. Fifth quadruple diffraction (Edif_q5) of the second considered NLOS scenario.

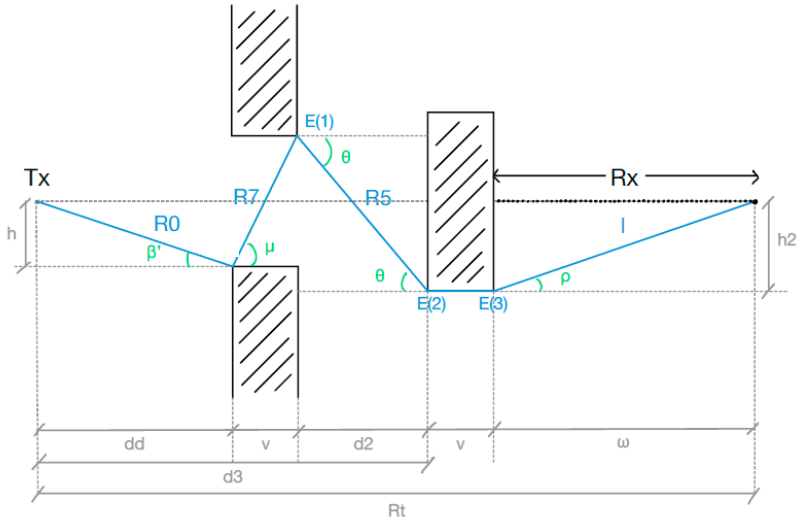

Figure 27. Sixth quadruple diffraction (Edif_q6) of the second considered NLOS scenario.

2.3.4. Total Signal

Regarding the above, the total signal at the receiver, taking into account all the contributions (including the additional symmetrical part of the street canyon), is

$$Et = 2(Edif\_d + Edif\_t1 + Edif\_t2 + Edif\_t3 + Edif\_q1 + Edif\_q2 + Edif\_q3 + Edif\_q4 + Edif\_q5 + Edif\_q6) \quad (65)$$

3. Results

This section presents the results obtained in the different scenarios considered using the GO/UTD formulations described above. We assume a frequency of 9.375 GHz, $E0 = 0.002555$, and vertical/*hard* polarization.

3.1. LOS Case

In this case, the parameters dd = 0.6 m, v = 0.03 m, and d2 = 0.8 m (when applicable) are considered. Figures 28 and 29 show the theoretical received power results (for one and two obstacles, respectively, and two values of h: 0.032 m and 0.05 m), calculated with the developed GO/UTD formulations, as a function of the distance from the transmitter. In addition, to compare the goodness of these results, the measurements presented in [8] for

the same scenarios and parameters are included in the figure. Additionally, for comparison purposes, the curves obtained with the PEM-RCNBC method are also shown in the plots.

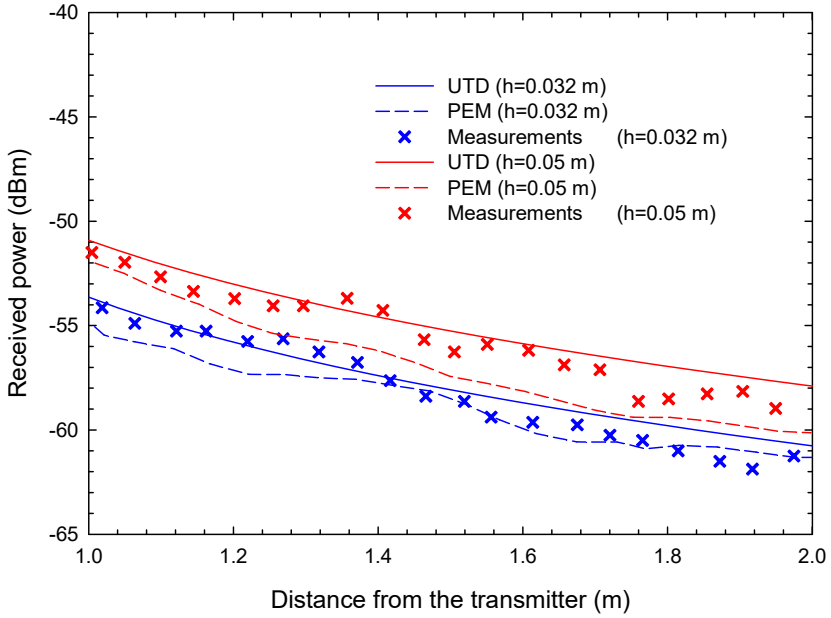

Figure 28. Comparison between the theoretical GO/UTD results for the LOS case (one obstacle) and the measurements presented in [8].

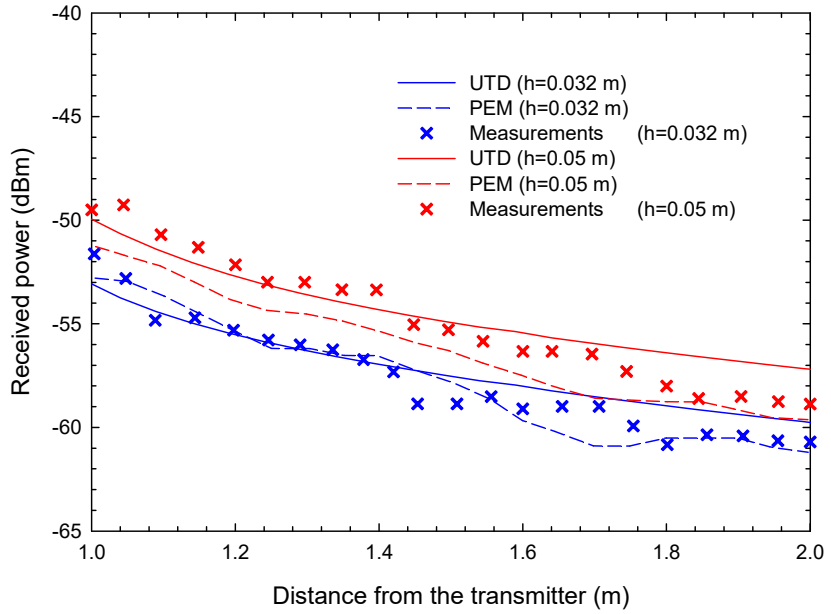

Figure 29. Comparison between the theoretical GO/UTD results for the LOS case (two obstacles) and the measurements presented in [8].

3.2. First NLOS Case

In this first NLOS case, the parameters dd = 0.42 m, v = 0.03 m, d2 = 0.92 m (when applicable), and h = 0.0375 m are considered. Thus, Figure 30 shows the theoretical results of received power for one and two obstacles achieved with the GO/UTD formulations obtained as a function of the distance from the transmitter. In this case, to validate these results, the measurements presented in [7] for the same scenarios and parameters are included in the figure. Moreover, the values obtained with the PEM-RCNBC method are also included in the figure.

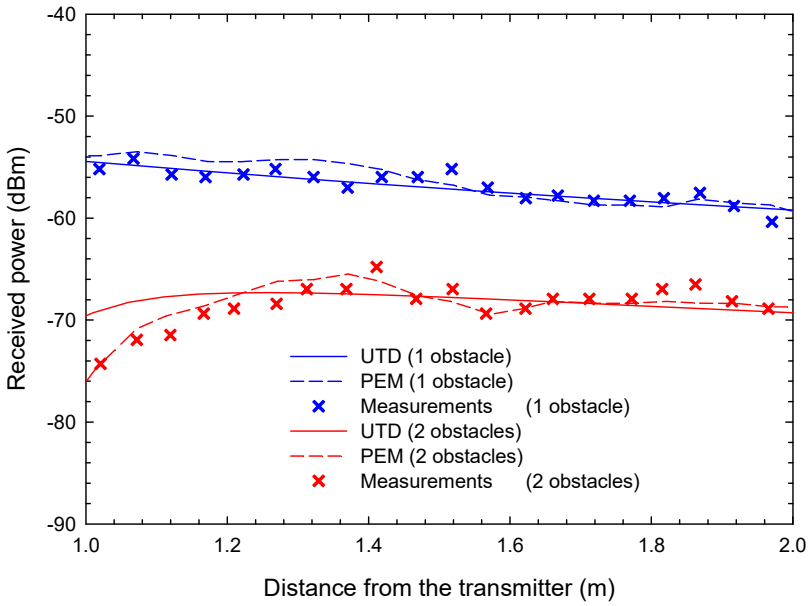

Figure 30. Comparison between the theoretical GO/UTD results for the first NLOS scenario and the measurements presented in [7].

3.3. Second NLOS Case

In the second NLOS scenario analyzed, the parameters dd = 0.6 m, d3 = 0.8 m, v = 0.03 m, h = 0.032 m, and h2 = 0.0375 m are considered. Thus, Figure 31 shows the theoretical received power results obtained with the developed GO/UTD formulations as a function of the distance from the transmitter. Additionally, in this case, in order to validate the results, the measurements presented in [7] for the same scenario and parameters are shown in the figure. On the other hand, the curve obtained with the PEM-RCNBC method has been included in the plot.

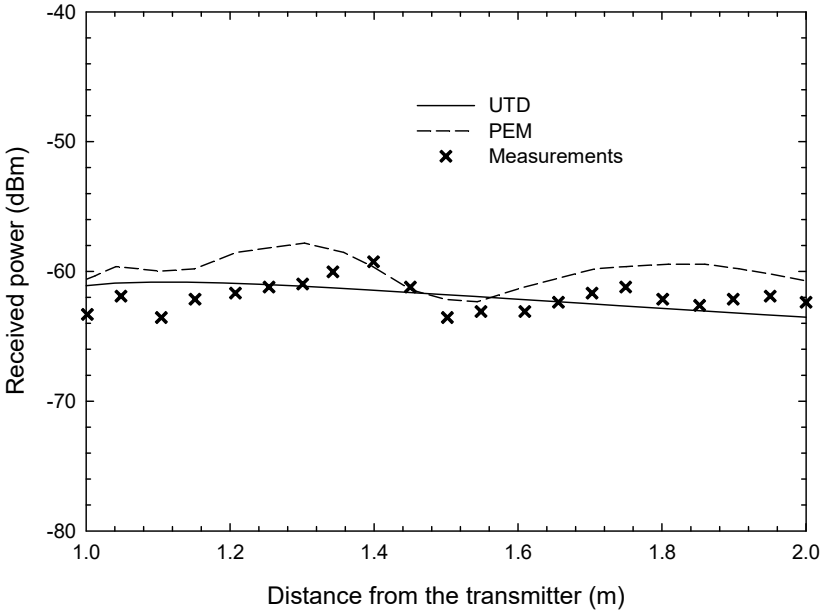

Figure 31. Comparison between the theoretical GO/UTD results for the second NLOS scenario and the measurements presented in [7].

3.4. Analysis of the Results

To further analyze the results presented in the previous subsections, Table 1 shows the mean error and variance between the theoretical and experimental data for all the cases considered (for both the UTD and PEM methods).

Table 1. Mean error and variance between the theoretical and experimental results presented in the previous subsections.

			Mean Error UTD (dB)	Mean Error PEM (dB)	Variance UTD (dB)	Variance PEM (dB)
LOS case	**1 obstacle**	**h = 0.032 m**	0.75	0.72	0.18	0.25
		h = 0.05 m	0.83	1.29	0.18	0.26
	2 obstacles	**h = 0.032 m**	0.81	0.64	0.33	0.31
		h = 0.05 m	0.92	1.32	0.30	0.30
First NLOS case	**1 obstacle**		0.65	1.00	0.28	0.35
	2 obstacles		1.45	0.83	1.73	0.44
Second NLOS case			1.09	2.07	0.47	0.88

As the table shows, the mean error obtained with the UTD method proposed in this work is lower than that achieved by the PEM solution in most cases, while also showing a lower variance in general. These results demonstrate the good agreement between the proposed UTD method and the experimental measurements, thereby validating the solution presented in this paper for radio wave propagation analysis in urban street canyons.

Additionally, for the LOS case and with respect to the UTD results, the mean error increases as both h and the number of obstacles increase. This behavior could be explained by the fact that, as both parameters increase, it is possible that, at the experimental level, not all diffracted and reflected contributions arrive with a sufficiently strong signal to be considered. Therefore, the experimental curves show more pessimistic power results than the theoretical ones (where all contributions are considered). This phenomenon is especially noticeable when the distance from the transmitter increases. On the other hand, regarding the first NLOS case and the UTD results, the discrepancy observed between the theoretical and measured values at smaller distances from the transmitter, when considering two obstacles, may be due to experimental near-field considerations with respect to the second obstacle, where part of the field would be absorbed by the conducting object and a decreased power characteristic of the near field would be observed. In any case, it should be noted that there will always be some discrepancy between theoretical values and measurements because the former are always calculated under ideal conditions, while the latter are subject to both uncontrolled conditions and experimental errors that can influence the results.

4. Conclusions

In this work, a series of formulations based on GO and UTD have been developed to analyze the propagation of radio waves in three urban street canyon scenarios. The results obtained from these formulations (in the horizontal plane containing the transmitter and receiver) have been validated by comparison with experimental measurements and the PEM method, with the UTD method showing, in most cases, a lower mean error with respect to the experimental data than that achieved by the PEM solution while also achieving a lower variance in general. In this sense, it should be noted that the discrepancy between the UTD method proposed in this paper and the measurements grows when increasing the parameter h (for the LOS case) and the number of obstacles. In any case, in view of these results obtained, we can conclude that the use of GO/UTD-based formulations can contribute to a simpler and computationally more efficient planning of D2D mobile communication systems in which the propagation environment considered can be modeled as an urban street canyon comprising rectangular and equispaced buildings. Future work will focus on more complex scenarios with more than one street (to consider diffraction and

reflection from one street to another) as well as considering finitely conducting obstacles rather than perfectly conducting obstacles.

Author Contributions: Conceptualization, E.B.-O., I.R.-R. and J.-V.R.; methodology, E.B.-O., I.R.-R. and J.-V.R.; software, E.B.-O., I.R.-R. and J.-V.R.; validation, E.B.-O., I.R.-R., J.-V.R., L.J.-L. and D.P.-Q.; formal analysis, E.B.-O., I.R.-R. and J.-V.R.; investigation, E.B.-O., I.R.-R. and J.-V.R.; resources, E.B.-O., I.R.-R., J.-V.R., L.J.-L. and D.P.-Q.; data curation, E.B.-O., I.R.-R., J.-V.R., L.J.-L. and D.P.-Q.; writing—original draft preparation, E.B.-O., I.R.-R. and J.-V.R.; writing—review and editing, E.B.-O., I.R.-R., J.-V.R., L.J.-L. and D.P.-Q.; visualization, E.B.-O., I.R.-R., J.-V.R., L.J.-L. and D.P.-Q.; supervision, E.B.-O., I.R.-R., J.-V.R., L.J.-L. and D.P.-Q.; project administration, I.R.-R., J.-V.R. and L.J.-L.; funding acquisition, I.R.-R., J.-V.R. and L.J.-L. All authors have read and agreed to the published version of the manuscript.

Funding: This work was supported by the Ministerio de Ciencia e Innovación, Spain, under Grant PID2019-107885GB-C33.

Institutional Review Board Statement: Not applicable.

Informed Consent Statement: Not applicable.

Data Availability Statement: The data that support the findings of this study are available upon request from the corresponding author.

Conflicts of Interest: The authors declare no conflict of interest.

References

1. Lu, J.S.; Bertoni, H.L.; Chrysanthou, C.; Boksiner, J. Simplified path gain model for mobile-to-mobile communications in an urban high-rise environment. In Proceedings of the IEEE Sarnoff Symposium, Princeton, NJ, USA, 12–14 April 2010.
2. Sasaki, M.; Yamada, W.; Kita, N.; Sugiyama, T. Path Loss Model with Low Antenna Height for Microwave Bands in Residential Areas. *IEICE Trans.* **2013**, *96-B*, 1930–1944. [CrossRef]
3. Lee, J.; Chung, H.K.; Kim, M.D. Building Height Effects on Path Loss for Low Antenna Links in Urban Street Grid Environments. In Proceedings of the IEEE Asia Pacific Wireless Communication Symposium, Seoul, Korea, 22–23 August 2013.
4. Erceg, V.; Schilling, D.L.; Ghassemzadeh, S.; Li, D.; Taylor, M. Propagation modeling and measurements in an urban and suburban environment using broadband direct sequence spread spectrum. In Proceedings of the IEEE Vehicular Technology Society 42nd VTS Conference, 10–13 May 1992; Volume 1, pp. 10–13.
5. Erceg, V.; Rustako, A.J., Jr.; Roman, R.S. Diffraction around corners and its effects on the microcell coverage area in urban and suburban environments at 900 MHz, 2 GHz, and 6 GHz. *IEEE Trans. Veh. Technol.* **1994**, *43*, 762–766. [CrossRef]
6. Masui, H.; Ishii, M.; Sakawa, K.; Shimizu, H.; Kobayashi, T.; Akaike, M. Microwave path-loss characteristics in urban LOS and NLOS environments. In Proceedings of the IEEE VTS 53rd Vehicular Technology Conference, Spring 2001. Proceedings (Cat. No. 01CH37202), Rhodes, Greece, 6–9 May 2001; Volume 1, pp. 395–398.
7. Ge, Z.-Y.; Lu, G.; Xiao, H.-B.; Zeng, D.; Gheit, A. Horizontal Diffraction in Multiple Obstacles Using Parabolic Equation with Recursive Convolution Nonlocal Boundary Conditions. *Prog. Electromagn. Res. M* **2017**, *56*, 179–187. [CrossRef]
8. Ge, Z.; Xiao, H.; Lu, G.; Zeng, D. Horizontal diffraction based on parabolic equation with nonlocal boundary conditions. In Proceedings of the 2017 IEEE 5th International Symposium on Electromagnetic Compatibility (EMC-Beijing), Beijing, China, 28–31 October 2017; pp. 1–4. [CrossRef]
9. Greivenkamp, J.E. *Field Guide to Geometrical Optics*; SPIE: New York, NY, USA, 2004.
10. Kouyoumjian, R.G.; Pathak, P.H. A uniform geometrical theory of diffraction for an edge in a perfectly conducting surface. *Proc. IEEE* **1974**, *62*, 1448–1461. [CrossRef]
11. Luebbers, R.J. A heuristic UTD slope diffraction coefficient for rough lossy wedges. *IEEE Trans. Antennas Propag.* **1989**, *37*, 206–211. [CrossRef]